Symmetry Breaking Resulting from Long-Range Interactions in Out of Equilibrium Systems: Elastic Properties of Irradiated AgCu

D. Simeone[*]

CEA, DES, ISAS, DMN, Paris-Saclay, F-91191 Gif sur Yvette, France

P. Garcia

CEA, DES, IRESNE, DEC, F-13108 Saint Paul Lez Durance, France

C. O. Bacri

Université Paris-Saclay, CNRS/IN2P3, IJClab, 91405 Orsay, France

L. Luneville

CEA, DES, ISAS, DM2S, Paris-Saclay, F-91191 Gif sur Yvette, France

This work presents a consistent formulation of the phase-field approach to model the behavior of nonmiscible alloys under irradiation which includes elastic strain fields, an example of a long-range interaction. Simulations show that the spatial isotropy that is characteristic of radiation-induced patterns breaks down as a result of the elastic strain energy. The consequence of this is the emergence of superlattice structures under irradiation liable to modify macroscopic material properties. This approach is assessed against the experimental study of a AgCu alloy under irradiation: we compare our simulation results to measured solubility limits and Young moduli.

Self-organization and pattern formation have been widely observed in various systems far from equilibrium [1–3]. In contrast to patterning in equilibrium systems [1,4–6], predicting all possible nonequilibrium steady states and rationalizing conditions in which they appear still constitute substantial challenges [1,7]. Meeting these challenges has wide ranging implications for the development of new technologies in almost every field of science and engineering. For example, mesoscopic nonequilibrium patterns formed by precipitates constitute one of the main factors influencing mechanical properties of advanced multiphase materials.

In solid-state physics, the time evolution of numerous systems such as block copolymer melts, ferrofluids, and magnetic systems [8] can be described by a Cahn-Hilliard (CH) equation [9] also known as model B in the Halperin-Hohenberg classification [10]. Many studies [1,7] have highlighted the fact that long-range interactions resulting in strain [11] or electric fields [12] can substantially influence the microstructure at equilibrium. For instance, the elastic strain energy induced by coherent B-rich precipitates in nonmiscible AB alloys is responsible for decreasing the critical temperature T_c at which demixing occurs [13,14].

The CH equation is also extensively applied to model the formation of radiation-induced patterns [15,16]. Under irradiation, two antagonistic influences may combine to drive an alloy toward a particular steady state [17,18]: thermodynamic forces (chemical potentials in our case) which are conducive to demixion, on the one hand, and atomic recoils induced by the slowing down of incident particles, on the other hand, otherwise known as ballistic mixing [19], which have a tendency to homogenize the system. This latter phenomenon acts over a characteristic length scale of a few nanometers [20,21]. Nonequilibrium steady states resulting from a combination between short- (chemical potential) and intermediate-range (ballistic mixing) interactions lead to patterning [15,16,22]. The objective of this Letter is to address the question of the impact of directional, long-range interactions (of a few hundreds of nanometers) on out of equilibrium patterning. We focus in the present study on the effect of the elastic strain energy induced by the presence of coherent precipitates under irradiation.

Because atomic scale modeling such as molecular dynamics or kinetic Monte Carlo techniques are by construction constrained to finite size simulation boxes, a number of technical difficulties may arise when long-range interactions are relevant [1]. The phase-field method provides a quite unique framework for treating these interactions explicitly [14,23,24] and therefore appears as a potentially useful tool for studying their impact on out of equilibrium patterns.

Let c_0 be the atomic fraction of species B at T_c, c_{eq}^p (c_{eq}^m) the equilibrium atomic fraction of species B in the

precipitate (matrix), and $\theta(\mathbf{r}, t) = [c(\mathbf{r}, t) - c_0]/[c_{eq}^p - c_{eq}^m]$ the dimensionless scalar order parameter (OP) which is proportional to the local atomic fraction $c(\mathbf{r}, t)$ of species B in the AB alloy. By solving the modified CH equation, changes in the radiation-induced microstructure of the alloy may be modeled [16]:

$$\frac{\partial\theta(\mathbf{r}, t)}{\partial t} = \nabla^2 \frac{\delta\mathcal{L}[\theta]}{\delta\theta(\mathbf{r}, t)}, \qquad (1)$$

where the functional $\mathcal{L}[\theta]$ captures the dependence of $\theta(\mathbf{r}, t)$ to chemical potentials, ballistic mixing, and the elastic strain energy. We will see later that $\mathcal{L}[\theta]$ may be regarded as a Lyapunov functional, the minimization of which provides the steady state solutions to Eq. (1). The elastic strain energy $\mathcal{W}[\theta]$ associated with spatial variations of $\theta(\mathbf{r}, t)$ results from the crystal lattice mismatch between the radiation-induced coherent B-rich precipitates and the A-rich matrix. Because the timescales for thermal (t_T), ballistic (t_B), and elastic (t_W) relaxation processes in solids [25] differ by several orders of magnitude, they act upon the system independently of each other so that $\mathcal{L}[\theta]$ may be expressed as the sum of three contributions:

$$\mathcal{L}[\theta] = \mathcal{F}[\theta] + \mathcal{M}(T, \phi)\mathcal{G}_\mathcal{R}[\theta] + \mathcal{W}[\theta]. \qquad (2)$$

$\mathcal{F}[\theta]$ is a temperature dependent short-range free energy. It is modeled by the usual dimensionless Landau-Ginzburg functional $\mathcal{F}[\theta] = \int [\theta(\mathbf{r}, t)^4/4] - [\theta(\mathbf{r}, t)^2/2] + [|\nabla\theta(\mathbf{r}, t)|^2/2] d\mathbf{r}$ and captures the evolution of the chemical potential of the alloy in the absence of radiation. The functional $\mathcal{G}_\mathcal{R}[\theta] = \frac{1}{2}\int\int \theta(\mathbf{r}, t)g_R(\mathbf{r} - \mathbf{r}')\theta(\mathbf{r}', t)d\mathbf{r}d\mathbf{r}'$ models ballistic mixing. Its kernel $g_R(\mathbf{r}) \propto \exp(-\mathbf{r}/R)/r$ is a exponential-like potential [16] whose characteristic range R is of a few nanometers [20]. It is a function of the energy and the nature of the incident particle [19]. The term $\mathcal{M}(T, \phi) \propto t_T/t_B$ characterizes the relative contributions of thermal and ballistic processes [16]. The functional $\mathcal{W}[\theta] = \frac{1}{2}\int\int \theta(\mathbf{r}, t)g_\infty(\mathbf{r}, \mathbf{r}')\theta(\mathbf{r}', t)d\mathbf{r}d\mathbf{r}'$ describes the long-range elastic strain energy due to the presence of B-rich precipitates. These precipitates induce a state of strain characterized by the following eigenstrain tensor [26]: $\epsilon_{ij}^0(\mathbf{r}, t) = \epsilon^0\delta_{ij}\Delta\theta(\mathbf{r}, t)$ [$\Delta\theta(\mathbf{r}, t) = \theta(\mathbf{r}, t) - \bar\theta$]. $\epsilon^0 = [(a^A - a^B)(c_{eq}^p - c_{eq}^m)/\bar a]$ is a measure of the misfit between a B-rich precipitate and the A-rich matrix; $\bar a$, a^A, and a^B are lattice constants of a fictitious homogeneous alloy of composition $\bar\theta$ and pure A and B metals [1]. In addition to this, one must also take into account the modification of the elastic tensor resulting from local variations of $\theta(\mathbf{r}, t)$:

$$C_{ijkl}(\mathbf{r}, t) = \bar C_{ijkl} + \Delta C_{ijkl}\Delta\theta(\mathbf{r}, t), \qquad (3)$$

where $\bar C_{ijkl}$ is the elasticity tensor of a fictitious homogeneous system of average OP, $\bar\theta$. The elastic energy of this homogeneous system is chosen as the reference elastic strain energy. $\bar C_{ijkl}$ can be computed from *ab initio* techniques [27]. ΔC_{ijkl} is equal to $(C_{ijkl}^B - C_{ijkl}^A)(c_{eq}^p - c_{eq}^m)$, where C_{ijkl}^B (C_{ijkl}^A) is the elasticity tensor for pure B (pure A).

In the absence of an elastic strain energy contribution [16], i.e., when $\mathcal{W}[\theta]$ is negligible, as in the case of nonmiscible alloys exhibiting very small misfits, ballistic effects dominate if $\mathcal{M}(T, \phi) \gg 1$ and the alloy eventually ends up as a homogeneous solid solution. For $\mathcal{M}(T, \phi) \ll 1$, chemical effects dominate and B-rich precipitates indefinitely coarsen. For $\mathcal{M}(T, \phi) \propto 1$, B-rich precipitates will coarsen to a certain point and reach a typical stable size of a few nanometers [18]. As the fourth-order term $\theta(\mathbf{r}, t)^4/4$ in the Landau-Ginzburg free energy affects the amplitude of the OP only [28], information relative to its spatial modulations is contained in the quadratic part of $\mathcal{L}[\theta]$. In Fourier space, this term reduces to $\frac{1}{2}\int D(q)|\widehat{\Delta\theta}(\mathbf{q}, t)|^2[d\mathbf{q}/(2\pi)^3]$, where $D(q) = [-1 + q^2 + \mathcal{M}(T, \phi)\hat g_R(q)]$. $D(q)$ is isotropic, i.e., depends exclusively upon the modulus of $\mathbf{q}$, q. The minimization of $D(q)$ with respect to q provides the modulations of B-rich precipitates which exhibit a wavelength $2\pi/q_0$ ($[dD(q)/dq] = 0$ for $q = q_0$). In general [16], ground states of $\mathcal{L}[\theta]$ are degenerate and wave vectors define a sphere of radius q_0 in Fourier space [16], which produces an isotropic pattern in real space.

The question arises whether this pattern is modified by $\mathcal{W}[\theta]$. The total strain field in our heterogeneous material can be expressed as the sum of two contributions: the first is an average strain field produced by the load exerted on the domain boundary and the second is a local strain field resulting from the presence of coherent B-rich precipitates. In this study, all calculations are performed assuming a zero external load. The functional $\mathcal{W}[\theta]$ can be computed from linear elasticity theory and is influenced by $\theta(\mathbf{r}, t)$ through Eq. (3), but also by the displacement field $\mathbf{u}(\mathbf{r}, t)$ due to the eigenstrain tensor $\epsilon_{ij}^0(\mathbf{r}, t)$.

As the relaxation time associated with elastic effects (t_W) is much smaller than that associated with diffusion phenomena (t_T and t_B), the components of the elastic displacement field $u_i^{ss}(\mathbf{r})$ ($i = 1, 2, 3$) may always be treated as being in a stationary state and therefore satisfy the time-independent mechanical equilibrium equation [29]:

$$\int \sum_{l=1}^3 G_{il}^{-1}(\mathbf{r}, \mathbf{r}')u_l^{ss}(\mathbf{r}')d\mathbf{r}' = f_i(\mathbf{r}). \qquad (4)$$

G^{-1} is the inverse Green operator of the problem [29]. The matrix element, G_{il}^{-1} is expressed as $G_{il}^{-1} = \sum_{j,k=1}^3 \bar C_{ijkl}(\partial^2/\partial r_j\partial r_k) + \Delta C_{ijkl}(\partial/\partial r_j)[\Delta\theta(\partial/\partial r_k)]$. The right-hand side term of Eq. (4), $f_i = \sum_{j,k,l=1}^3 \epsilon^0\delta_{kl} \times \{\bar C_{ijkl}[\partial\Delta\theta(\mathbf{r}, t)/\partial r_j] + \Delta C_{ijkl}[\partial(\Delta\theta(\mathbf{r}, t)^2)/\partial r_j]\}$ has two contributions. The first is the eigenstrain tensor $\epsilon_{ij}^0(\mathbf{r}, t)$

resulting from the presence of B-rich precipitates and the second is a consequence of the local variations of $C_{ijkl}(\mathbf{r}, t)$. Solving Eq. (4) provides the displacement field $\mathbf{u}^{ss}(\mathbf{r})$ whence the elastic strain energy is derived. If no additional hypotheses are formulated, the solution to Eq. (4) can only be obtained numerically [24].

In order to derive an analytical solution for understanding how the elastic strain energy influences microstructural changes under irradiation, we assume that the interface between a precipitate and the matrix is abrupt. The implication is that $[\partial(\Delta\theta(\mathbf{r}, t))^2/\partial r_j] \approx 2\omega[\partial(\Delta\theta(\mathbf{r}, t))/\partial r_j]$, which makes f_i a linear function of $[\partial(\Delta\theta(\mathbf{r}, t))/\partial r_j]$ $[\omega = \{[(\max(\theta(\mathbf{r}, t)) + \min(\theta(\mathbf{r}, t)))/2] - \bar{\theta}\}$ is the difference between the local and global average values of $\theta(\mathbf{r}, t)]$. This allows us to establish an explicit expression for $\mathcal{W}[\theta]$ since $\mathbf{u}^{ss}(\mathbf{r})$ can be analytically computed from Eq. (4) [29]:

$$\mathcal{W}[\theta] = \frac{1}{2}\iint \hat{g}_\infty(\mathbf{q}, \mathbf{q}')\hat{\Delta\theta}(\mathbf{q}, t)\overline{\hat{\Delta\theta}}(\mathbf{q}', t)\frac{d\mathbf{q}}{(2\pi)^3}\frac{d\mathbf{q}'}{(2\pi)^3}, \quad (5)$$

where $\widehat{\Delta\theta}(\mathbf{q}, t)$ is the Fourier transform of $\Delta\theta(\mathbf{r}, t)$ and $\overline{\widehat{\Delta\theta}}(\mathbf{q}, t)$ denotes the complex conjugate of $\widehat{\Delta\theta}(\mathbf{q}, t)$. $\hat{g}_\infty(\mathbf{q}, \mathbf{q}') = \sum_{i,j=1}^{3} \bar{\sigma}_i(\mathbf{q})\hat{G}_{ij}(q, q')\sigma_j(\mathbf{q}')$, is the Fourier transform of $g_\infty(\mathbf{r}, \mathbf{r}')$, where $\sigma_i(\mathbf{q}) = \mathbf{i}\sum_{j,k,l=1}^{3} q_j(\bar{C}_{ijkl} + \Delta C_{ijkl}\omega)\epsilon^0\delta_{kl}$ ($\mathbf{i}^2 = -1$). Cauchy's principal value $\int$ must be used to compute $\mathcal{W}[\theta]$ as $\hat{g}_\infty(\mathbf{q}, \mathbf{q}')$ is singular at $\mathbf{q} = 0$ (elastic interactions have an infinite range). The key point here is that $g_\infty(\mathbf{r}, \mathbf{r}')$ is a function of vectors $\mathbf{r}$ and $\mathbf{r}'$. The elastic strain energy $\mathcal{W}[\theta]$ is therefore anisotropic, in contrast to $\mathcal{F}[\theta]$ and $\mathcal{G}_R[\theta]$. Note that numerical calculations [24,30] have demonstrated the anisotropic character of $\mathcal{W}[\theta]$ in the case of smooth interfaces also.

Equation (5) provides the last expression necessary to calculate $\mathcal{L}[\theta]$. Since $|\theta| < 1$, $\mathcal{L}[\theta]$ has a lower bound. In addition, it is a decreasing function of time and so may be seen as a Lyapounov functional for Eq. (1). Steady states of Eq. (1) are therefore obtained from the minimization of $\mathcal{L}[\theta]$ with the constraint that $(1/\Omega)\int \theta(\mathbf{r}, t)dr = \bar{\theta}$. They are anisotropic as they must minimize $\mathcal{L}[\theta]$ along specific directions corresponding to minima of $\mathcal{W}[\theta]$ and this induces the formation of B-rich precipitate superlattices. It is a phenomenon that requires no energy and is induced by Goldstone modes [31] as observed in liquid to solid transitions.

To go one step beyond, $\mathcal{W}[\theta]$ and therefore $G(\mathbf{r}, \mathbf{r}')$ need to be computed. The inverse Green operator may be written as

$$G_{il}^{-1} = \sum_{j,k=1}^{3} \bar{C}_{ijkl}\left[\frac{\partial^2}{\partial r_j\partial r_k} + \frac{\Delta C_{ijkl}}{\bar{C}_{ijkl}}\frac{\partial}{\partial r_j}\left(\Delta\theta\frac{\partial}{\partial r_k}\right)\right]$$
$$= (G_0^{-1})_{il} + V_{il}. \quad (6)$$

G_0^{-1} is associated with the homogeneous elasticity tensor $\bar{C}_{ijkl}$ and V which is proportional to $\Delta C_{ijkl}/\bar{C}_{ijkl}$ constitutes a perturbation term which captures the variations of the elastic tensor due to the formation of B-rich precipitates. The Dyson equation $(G = G_0 - G_0VG)$ provides an expression for G which may further be written as an analytical series expansion of operators G_0 and V: $G = \sum_{p=0}^{\infty}(-1)^p(G_0V)^pG_0$ [29]. Replacing G by its expansion in Eq. (5) provides an expression for $\mathcal{W}[\theta]$ in the form of an infinite series, the general term of which is $\mathcal{W}_p[\theta]$.

We have applied this theoretical approach to the study of irradiated AgCu cubic alloys which exhibit a large eigenstrain tensor ($\epsilon^0 \approx 0.10$). Based on the knowledge of the elastic constants for Ag and Cu [32], the convergence radius of the series expansion of G may be estimated. It is proportional to $(\Delta C_{2323}/\bar{C}_{2323})$ and therefore remains always lower than 1, thus proving the convergence of the series. Moreover, $\mathcal{W}_p[\theta] \propto (\Delta C_{2323}/\bar{C}_{2323})^p\mathcal{W}_0[\theta]$ decreases rapidly; e.g., $\mathcal{W}_1/\mathcal{W}_0 = 0.26$ and $\mathcal{W}_2/\mathcal{W}_0 = 0.08$. It therefore appears to be necessary and sufficient to use a first-order expansion of $\mathcal{W}[\theta]$ (i.e., including terms $\mathcal{W}_0[\theta]$ and $\mathcal{W}_1[\theta]$ only) to model radiation-induced patterning adequately. The zero-order elastic strain energy contribution to $\mathcal{L}[\theta]$ represents approximately 8% of the free energy: $W_0/\mathcal{F}_0 = [\bar{C}_{2323}(\epsilon^0)^2/\mathcal{F}_0] \approx 0.08$. This high ratio shows that the AgCu alloy is particularly sensitive to elastic strains within the range of temperatures we have studied. Equation (1) is solved numerically assuming periodic and zero-flux boundary conditions [$\nabla\theta(\mathbf{r}, t) = 0$ on domain boundary $\delta\Omega$]. Based on Eyre's work [33], a semi-implicit unconditionally stable scheme can be set up in Fourier space. This is done by expressing $\mathcal{L}[\theta]$ as the difference between contracting (the quadratic part of $\mathcal{F}[\theta]$, $\mathcal{G}_\mathcal{R}[\theta]$, and $W_0[\theta]$) and expansive (the nonquadratic quadratic part of $\mathcal{F}[\theta]$ and $W_1[\theta]$) contributions. Coefficients of the Landau expansion $a_2(T)$, $a_3(T)$, and $a_4(T)$ are obtained from fitting the AgCu equilibrium phase diagram [34]. The stiffness term related to the width of precipitate-matrix interfaces was estimated at 1.5 eV nm^{-1} from Monte Carlo simulations [35]. The characteristic length for ballistic mixing R (0.3 nm) was determined assuming a binary collision approximation [35]. Refer to Ref. [36] for details. Silver and copper atoms are initially randomly distributed as the alloy temperature lies above T_c. This provides the initial conditions for the OP.

Figure 1 shows steady state microstructures of an Ag$_{0.42}$Cu$_{0.58}$ irradiated sample as computed from Eq. (1). The introduction of an elastic strain energy is responsible for a drastic modification of the microstructure. In the absence of this contribution, the calculation indicates the emergence of a pattern [see Fig. 1(a)] which is isotropic in $\mathbf{q}$ space [see Fig. 1(d)]. Accounting for the zero-order elastic term W_0 destabilizes this pattern and induces an ordered superlattice of stripes [see Figs. 1(b) and 1(e)].
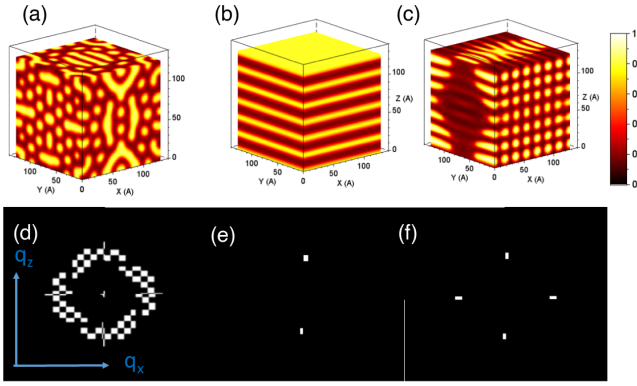
FIG. 1. Calculated steady state modulations of the silver concentration in $Ag_{0.42}Cu_{0.58}$ samples irradiated with 1.6 MeV Kr ions at $T = 443$ K (flux of 6×10^{11} cm^{-2} s^{-1}). These microstructures are computed for different contributions of the elastic strain energy [(a) $W_0 = 0$ and $W_1 = 0$ (no contribution), (b) $W_0 \neq 0$ and $W_1 = 0$ (zero-order expansion of elastic strain energy), (c) $W_0 \neq 0$ and $W_1 \neq 0$ (first-order expansion of elastic strain energy)] and exhibit quite different characteristics. The formation of ordered superlattices of precipitates occurs when an elastic interaction is modeled, as illustrated by the Fourier transforms [(d) $W_0 = 0$ and $W_1 = 0$, (e) $W_0 \neq 0$ and $W_1 = 0$, (f) $W_0 \neq 0$ and $W_1 \neq 0$].

Addition of the first-order term W_1 produces a stable microstructure which is a two-dimensional superlattice of B-rich rods [see Figs. 1(c) and 1(f)]. The characteristic size of these rods is roughly 5 nm, in line with experimental observations [18,37,38] and with the fact that precipitates are coherent. Figure 1(c) and its associated Fourier transform Fig. 1(f) show that the elastic energy contribution induces a condensation of wave vectors along specific directions, thus destroying the originally isotropic pattern illustrated in Figs. 1(a) and 1(d).

We now endeavor to illustrate through comparison to experimental data the relevance of the theory exposed above. Assessment of the model is carried out against two types of data: solubility limits and Young moduli pertaining to $Ag_{0.42}Cu_{0.58}$ samples irradiated at various temperatures with a 6×10^{11} cm^{-2} s^{-1} flux of 1.6 MeV krypton ions to a fluence of 2×10^{16} cm^{-2}, thus ensuring that steady states are reached [37]. Five thin-film samples were prepared using plasma vapor deposition on (100) silicon single crystal wafers. The thin-film thickness was chosen so that the damage it sustained was homogeneous and to guarantee that the krypton ions were not implanted in the thin film. Ion irradiations were carried out at the SCALP facility [39]. Solubility limits have already been reported in a previous Letter [16], whereas Young moduli constitute original data. Experimental solubility limits reported in Fig. 2 were obtained from a room temperature, grazing incidence, x-ray diffraction characterization of irradiated samples. The incidence angle of x rays (1°) was chosen to maximize the intensity of diffraction patterns. The full pattern analysis of diagrams provided values for lattice parameters
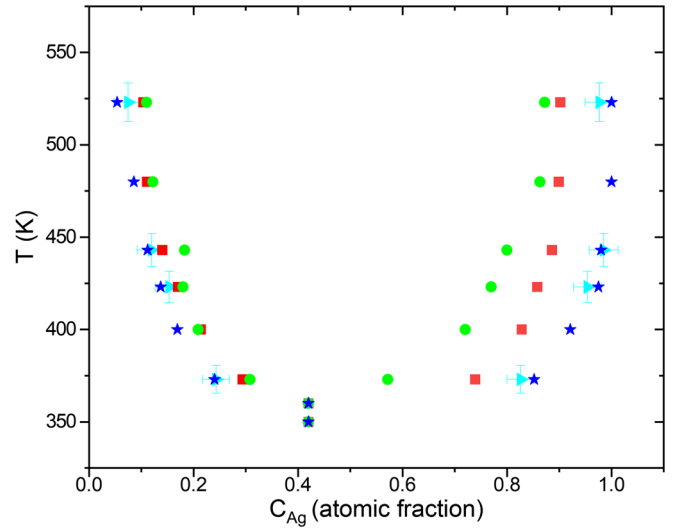

FIG. 2. Comparison between experimental solubility limits (cyan triangles) of Ag in irradiated $Ag_{0.42}Cu_{0.58}$ thin films at different temperatures and computed from Eq. (1) [$W_0 = W_1 = 0$, red squares; $W_0 \neq 0$ and $W_1 = 0$, full green circles; $W_0 \neq 0$ and $W_1 \neq 0$, blue stars].

of the matrix and precipitates, whence solubility limits were derived [40] ($R_{wp} < 5\%$ for all patterns). Figure 2 shows that W_0 and W_1 terms of the $\mathcal{W}[\theta]$ expansion must be included in the calculation to reproduce the experimental data satisfactorily.

The irradiated samples' Young moduli were determined from nanoindentation experiments carried out at room temperature using a modified Berkovich tip. The reduced moduli were obtained from the analysis of load-displacement curves collected using the multiple-point method [41]. For each indentation test, the load was increased linearly between 0 and 5 mN. However, in addition, a dynamical method was implemented which involved superimposing a low amplitude (0.5 mN), 20 Hz oscillatory motion of the indenter as it penetrated the material [41]. This enabled us to measure a large number of data under a single indent. Assuming a Poisson ratio of 0.24 for all irradiated thin films in agreement with our phase-field simulations (see below), the Young modulus for each thin film can be determined from the knowledge of the reduced Young moduli [41]. These Young moduli are shown in Fig. 3 as a function of irradiation temperature.

The corresponding simulated values were obtained as follows. The effective elasticity tensor C_{ijkl}^{eff} was explicitly calculated from the second derivative of the Lyapounov functional with respect to the average strain tensor:

$$C_{ijkl}^{\mathrm{eff}} = \bar{C}_{ijkl} - \Delta C_{ijrs} A_{rstu} \Delta C_{tukl},$$

$$A_{rstu} = -\frac{1}{V} \iint \hat{g}_\infty(\mathbf{q},\mathbf{q}') \widehat{\Delta\theta}(\mathbf{q},t) \overline{\widehat{\Delta\theta}(\mathbf{q}',t)} \frac{d\mathbf{q}}{(2\pi)^3} \frac{d\mathbf{q}'}{(2\pi)^3}. \quad (7)$$

The Young modulus and Poisson ratio of a polycrystalline sample are computed by averaging C_{ijkl}^{eff} [i.e., Eq. (7)] over
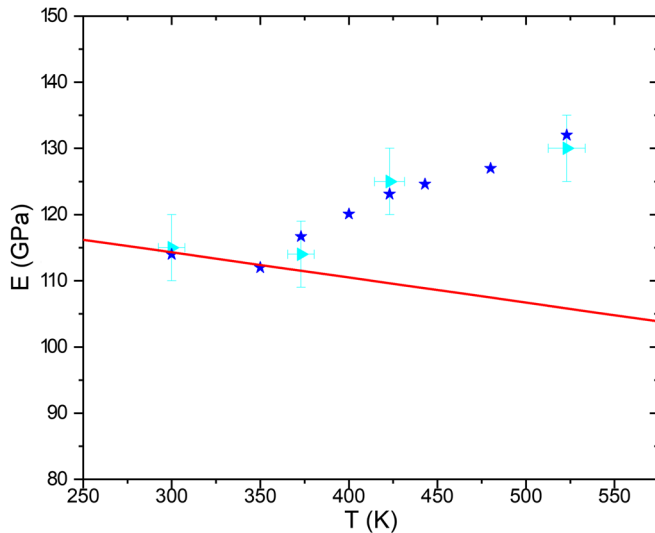
FIG. 3. Comparison between calculated and experimental irradiation temperature dependent Young moduli. Two simulation results are reported, both of which were obtained from the minimization of $\mathcal{L}[\theta]$. The first (red line) concerns calculations for which only the chemical potential and ballistic mixing contributions to the Lyapounov were taken into account. The second (blue stars) concerns calculations for which chemical potential, ballistic mixing, and elastic contributions were modeled. The experimental data are obtained from nanoindentation experiments on irradiated $Ag_{0.42}Cu_{0.58}$ thin films (cyan triangles).

all crystalline directions [42]. The calculated Poisson ratio was found to be insensitive to irradiation temperature and remained equal to 0.24. The computed effective Young moduli reproduce the experimental data remarkably well (Fig. 3). In addition, one notes that in the absence of an elastic strain energy contribution (red line in Fig. 3), the Young's modulus is a decreasing function of temperature. This demonstrates that the experimentally measured increase of the Young modulus with irradiation temperature results from elastic effects alone. Further, one may surmise that point defects have no significant influence on the Young modulus, since if this were not the case, one would expect the Young modulus to be a decreasing function of the irradiation temperature, as higher temperatures are conducive to defect elimination.

To conclude, we demonstrate in this work that microstructural changes under irradiation in AgCu alloys may be modeled adequately using the phase-field method, on the condition that zero- and first-order contributions of the elastic strain energy be modeled. It is shown that the spatial isotropy that is characteristic of patterns in the absence of an elastic strain energy contribution to the Lyapounov functional disappears when elastic effects are taken into account. The consequence of this is the emergence of superlattices under irradiation. On a more general note, we provide an example of how to compute an essential but complex material property via a multiscale approach. Atomic scale methods alone cannot provide such

information due to the long-range nature of elastic interactions. By its ability to take these interactions into account in systems maintained far from equilibrium, such an approach could be applied for instance to the study of mixed oxide nuclear fuels [43].

*david.simeone@cea.fr

[1] N. Ghoniem and D. Walgraef, *Instabilities and Self Organization in Materials* (Oxford Science Publications, New York, 2008), Vol. I.
[2] D. Simeone, J. Ribis, and Luneville, Continuum approaches for modeling radiation-induced self-organization in materials: From the rate theory to the phase field approach, J. Mater. Res. **33**, 440 (2018).
[3] M. W. Noble, M. R. Tonks, and S. P. Fitzgerald, Turing Instability in the Solid State: Void Lattice in Irradiated Metals, Phys. Rev. Lett. **124**, 167401 (2020).
[4] G. Van kampen, *Processes in Physics and Chemistry* (North-Holland, Amsterdam, 1980).
[5] G. Nicolis and I. Prigogine, *Self Organization in Nonequilibrium Systems: From Dissipative Structure to Order through Fluctuations* (Wiley, New York, 1977).
[6] M. Cross and H. Greenside, *Pattern Formation and Dynamics in Nonequilibrium Systems* (Cambridge University Press, Cambridge, England, 2009).
[7] B. Bergersen and Z. Racz, Dynamical Generation of Long-Range Interactions: Random Levy Flights in Kinetic Ising and Spherical Models, Phys. Rev. Lett. **67**, 3047 (1991).
[8] M. Seul and D. Andelman, Domain shapes and patterns: The phenomenology of modulated phases, Science **267**, 476 (1995).
[9] J. W. Cahn and J. E. Hilliard, Free energy of a nonuniform system. I. Interfacial free energy, J. Chem. Phys. **28**, 258 (1958).
[10] P. C. Hohenberg and B. I. Halperin, Theory of dynamic critical phenomena, Rev. Mod. Phys. **49**, 435 (1977).
[11] J. W. Cahn, Phase separation by spinodal decomposition in isotropic systems, J. Chem. Phys. **42**, 93 (1965).
[12] S. Semenovskaya and A. G. Katchaturyan, Ferrelectric transition in a random field: Possible relaxation to relaxor ferroelectrics, Ferroelectrics **206–207**, 157 (1998).
[13] J. Cahn, Hardening by spinodal decomposition, Acta Metall. **11**, 1275 (1963).
[14] A. G. Khatchaturyan, *Theory of Structural Transformation in Solids* (Wiley Interscience, New York, 1983).
[15] R. A. Enrique and P. Bellon, Compositional Patterning in Systems Driven by Competing Dynamics of Different Length Scale, Phys. Rev. Lett. **84**, 2885 (2000).
[16] L. Luneville, P. Garcia, and D. Simeone, Predicting Nonequilibrium Patterns beyond Thermodynamic Concepts:

Application to Radiation-Induced Microstructures, Phys. Rev. Lett. **124,** 085701 (2020).

[17] G. Martin, Phase stability under irradiation: Ballistic effects, Phys. Rev. B **30,** 1424 (1984).

[18] D. Simeone, G. Demange, and L. Luneville, Disrupted coarsening in complex Cahn-Hilliard dynamics, Phys. Rev. E **88,** 032116 (2013).

[19] P. Sigmund and A. Gras-Marti, Theoretical aspects of atomic mixing by ion beams, Nucl. Instrum. Methods Phys. Res., Sect. B **182,** 211 (1981).

[20] K. Nordlund and R. S. Averback, Role of Self-Interstitial Atoms on the High Temperature Properties of Metals, Phys. Rev. Lett. **80,** 4201 (1998).

[21] G. Demange, E. Antoshchenkova, M. Hayoun, L. Luneville, and D. Simeone, Simulating the ballistic effects of ion irradiation in the binary collision approximation: A first step toward the ion mixing framework, J. Nucl. Mater. **486,** 26 (2017).

[22] L. Luneville, K. Mallick, V. Pontikis, and D. Simeone, Patterning in systems driven by nonlocal external forces, Phys. Rev. E **94,** 052126 (2016).

[23] J. W. Cahn, On spinodal decomposition, Acta Metall. **9,** 795 (1961).

[24] S. Hu, S. Wei, and L. Chen, Phase field model for evolving microstructures with strong elastic inhomogeneities, Acta Metall. **49,** 1879 (2001).

[25] P. Stefanovic, M. Haataja, and N. Provatas, Phase-Field Crystals with Elastic Interactions, Phys. Rev. Lett. **96,** 225504 (2006).

[26] J. Eshelby, in *Progress in Solid Mechanics,*, 2nd ed., edited by I. N. Sneddon and R. Hill (North-Holland, Amsterdam, 1961).

[27] A. Zunger, S. H. Wei, L. G. Ferreria, and J. E. Bernard, Special Quasirandom Structures, Phys. Rev. Lett. **65,** 353 (1990).

[28] M. C. Cross and P. C. Hohenberg, Pattern formation outside of equilibrium, Rev. Mod. Phys. **65,** 851 (1993).

[29] A. G. Katchaturyan, S. Semenovskaya, and T. Tsakalakos, Elastic strain energy in inhomogeneous solids, Phys. Rev. B **52,** 15909 (1995).

[30] S. Hu and L. Cheng, A phase field model for evolving microstructures with strong elastic inhomogeneity, Acta Mater. **49,** 1879 (2001).

[31] J. Goldstone, Field theories with superconductor solutions, Nuovo Cimento **19,** 154 (1961).

[32] Y. Chang and L. Himmel, Temperature dependence of the elastic constants of Cu, Ag, and Au above room temperature, J. Appl. Phys. **37,** 3567 (1966).

[33] D. J. Eyre, Unconditionally gradient stable time marching the Cahn-Hilliard equation, MRS Proc. **529,** 39 (1998).

[34] P. Subramanian and J. Perepezko, The Ag-Cu system: A phase diagram evaluation, J. Phase Equilib. **14,** 62 (1993).

[35] G. Demange, L. Luneville, V. Pontikis, and D. Simeone, Prediction of irradiation induced microstructures using a multiscale method coupling atomistic and phase field modeling: Application to the AgCu model alloy, J. Appl. Phys. **121,** 125108 (2017).

[36] G. Demange, Mise en oeuvre d'une approche multi-echelle fondée sur le champ de phase pour caractériser la microstructure des matériaux irradiés: Application a l'alliage AgCu, Ph. D. thesis, Université Paris Sud-Paris XI, 2015.

[37] S. Chee, B. Stumphy, N. Vo, R. Averback, and P. Bellon, Dynamic self-organization in Cu alloys under ion irradiation, Acta Mater. **58,** 4088 (2010).

[38] L. Q. Chen and A. G. Khatchaturyan, Dynamics of Simultaneous Ordering and Phase Separation and Effect of Long Range Coulomb Interactions, Phys. Rev. Lett. **70,** 1477 (1993).

[39] C.-O. Bacri, C. Bachelet, C. Baumier, J. Bourçois, L. Delbecq, D. Ledu, N. Pauwels, S. Picard, S. Renouf, and C. Tanguy, SCALP: A platform dedicated to material modifications and characterization under ion beam, Nucl. Instrum. Methods Phys. Res., Sect. B **406,** 48 (2017).

[40] B. Tsaur, S. Lau, and J. Mayer, Continuous series of metastable AgCu solid solutions formed by ion beam mixing, Appl. Phys. Lett. **36,** 823 (1980).

[41] A. Fiscker-Cripps, *Nanoindentation* (Springer Science, New York, 2004).

[42] S. Meille and E. Garboczi, Linear elastic properties of 2D and 3D models of porous materials made from elongated objects, Model. Simul. Mater. Sci. Eng. **9,** 371 (2001).

[43] D. Simeone, J.-M. Costantini, L. Luneville, L. Desgranges, P. Trocellier, and P. Garcia, Characterization of radiation damage in ceramics: Old challenge new issues?, J. Mater. Res. **30,** 1495 (2015).